Laser and Particle Beams (2001), *19*, 67–73. Printed in the USA.

Single-shot spectral interferometry of femtosecond laser-produced plasmas

S. REBIBO,[1] J.-P. GEINDRE,[1] P. AUDEBERT,[1] G. GRILLON,[2] J.-P. CHAMBARET,[2] AND J.-C. GAUTHIER[1]

[1]Laboratoire pour l'Utilisation des Lasers Intenses, UMR 7605 CNRS—Ecole polytechnique—CEA—Université Paris VI, Ecole polytechnique, 91128 Palaiseau, France
[2]Laboratoire d'Optique Appliquée, UMR 7639 CNRS—ENSTA—Ecole polytechnique, Batterie de l'Yvette, 91761 Palaiseau, France

(RECEIVED 5 December 2000; ACCEPTED 5 February 2001)

Abstract

We use both a Fourier-transform-based analysis and time-retrieval calculations to get time-resolved measurements of the reflectivity and the phase shift of a chirped probe pulse interacting with a fs-laser-produced plasma by spectral interferometry in a single shot. We have devised a novel dual-quadrature Mach–Zehnder configuration in which wavefront division is used to obtain spatial fringes from the perturbed and unperturbed probe simultaneously. We demonstrate the capability of this technique with fully analyzed experimental data on the interaction of a femtosecond laser with C_3H_6 and C samples, showing 35-fs time resolution.

1. INTRODUCTION

Fourier-Domain Interferometry (FDI) is a well-established linear optical technique to retrieve the phase and amplitude of an unknown electric field $E(t)$ in the femtosecond time domain (Froehly *et al.*, 1973; Piasecki *et al.*, 1980; Tokunaga *et al.*, 1992). More precisely, femtosecond spectral interferometry provides a measurement of the Fourier transform of the electric field, $E(\omega)$, in both amplitude and phase (Geindre *et al.*, 1994; Lepetit *et al.*, 1995), by comparison with a known field, $E_0(\omega)$. This technique is now widely used in ultrafast laser-matter interaction experiments including molecular spectroscopy (Scherer *et al.*, 1991), femtosecond laser-induced shock waves (Evans *et al.*, 1996), laser-induced dielectric damage (Audebert *et al.*, 1994; Guizard *et al.*, 1995), and laser wake-field particle acceleration (Marquès *et al.*, 1996; Siders *et al.*, 1996), to name a few. Dual-quadrature spectral interferometry, in which the phase and amplitude perturbation of a weak probe field are measured simultaneously in S- and P-polarizations, has been applied in plasma physics to measure time-resolved ionization and plasma expansion (Blanc *et al.*, 1996; Quoix *et al.*, 1999, 2000) following laser interaction.

In spectral interferometry, the perturbed laser pulse to be characterized is set up to interfere with a reference pulse in a spectrometer, yielding spectral fringes of period inversely proportional to the optical path difference between the two beams, which in turn depends on the phase. However, one drawback of spectral interferometry is that a complete time history of the perturbation under study can be obtained only with multiple shots (Geindre *et al.*, 1994). One way of solving this problem consists of using a chirped probe, giving a univocal relation between the instantaneous frequency and time to encode the pulse spectrum with the time history of the perturbation. Along these lines, chirped-pulse reflectometry was proposed for laser-produced shock breakout measurements (Gold *et al.*, 1996) and twin-chirped-pulse FDI was implemented with picosecond time resolution in shock wave studies (Benuzzi-Mounaix *et al.*, 1999) and laser-induced breakdown of air (Chien *et al.*, 1999).

In this paper, we present a new implementation of single-shot chirped-pulse FDI which uses wavefront and quadrature polarization division in the two arms of a Mach–Zehnder interferometer. We also discuss the question of the ultimate time resolution which can be achieved with such a technique. When a linear chirp is applied to the probe pulse, we demonstrate that the temporal resolution is not defined by the time scale between adjacent fringes (Chien *et al.*, 1999) but is determined by the simultaneous fulfillment of the Fourier time-bandwidth product and the linear relation

Address correspondence and reprint requests to: Jean-Claude Gauthier, Directeur-Adjoint du LULI, LULI, Ecole Polytechnique, Route de Saclay, 91128 Palaiseau, France,. E-mail: jean-claude.gauthier@polytechnique.fr

between frequency and time. We propose a reconstruction procedure which allows us to process single-shot spectral interferograms to obtain time-resolved amplitude and phase simultaneously in S- and P-polarization with a temporal resolution limited only by the spectral bandwidth of the probe pulse. We demonstrate the usefulness of this technique in laser-induced dielectric breakdown and in the characterization of the electron density gradient scale length in controlled-prepulse laser-target interaction experiments.

2. EXPERIMENTAL TECHNIQUE AND SETUP

Single-shot FDI measurements rely on the use of positive or negative linearly chirped pulses. With chirped-pulse amplification (CPA) lasers (Strickland & Mourou, 1985), such a pulse is easily obtained by slightly translating one of the compressor gratings from its original position. The spectral bandwidth of the pulse is not modified but the pulse duration is lengthened. The instantaneous frequency varies with time according to a linear law:

$$\omega(t) = \omega_0 + at, \tag{1}$$

where ω_0 is the central frequency of the laser and $a = 1/\Phi^{(2)}(\omega_0)$ is the inverse of the quadratic phase. Accordingly, the time range over which single-shot measurements can be made is roughly $\Delta t \approx \Delta\Omega \times \Phi^{(2)}(\omega_0)$ where $\Delta\Omega$ is the full width at half maximum (FWHM) pulse bandwidth.

2.1. Temporal resolution

Because there is a linear relation between frequency and time (see Fig. 1), a phase and amplitude perturbation of duration δt in the time domain gives rise to a perturbation of spectral bandwidth $\Delta\omega = a \times \delta t$ in the frequency domain. For a Gaussian pulse, the FWHM duration ΔT of the chirped pulse, in intensity, is

$$\Delta T = \Delta T_0 \sqrt{1 + \frac{[4 \ln 2 \Phi^{(2)}(\omega_0)]^2}{(\Delta T_0)^4}}, \tag{2}$$

where ΔT_0 is the original duration of the pulse. In the case of a perturbation duration which is significant with respect to ΔT (see the pulse at the right of the time axis in Fig. 1), the Fourier Time-bandwidth product relation gives a frequency perturbation of width $d\omega_2 \geq (4 \ln 2)/(\delta t_2)$, which is much smaller than the bandwidth $\Delta\omega_2$ determined from the linear chirp. The perturbation in the frequency domain can be said to be "localized" inside this bandwidth. By combining the time-bandwidth product and the linear chirp, one obtains a value of the minimum perturbation duration δt for which the linear chirp bandwidth is comparable to the Fourier bandwidth:

$$\delta t^2 \geq \frac{4 \ln 2}{a} \tag{3}$$

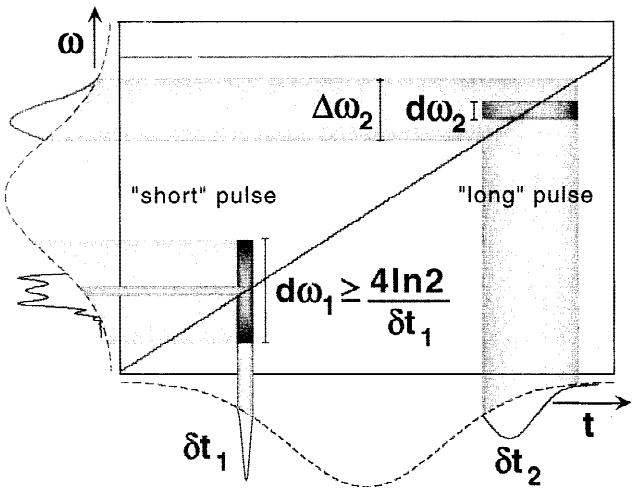

Fig. 1. Time-frequency plot showing the linear chirp relation and the frequency extent of a short temporal perturbation (left) and a long temporal perturbation (right). The dashed curve below the time axis gives the Gaussian temporal shape of the chirped pulse of FWHM ΔT. The dashed curve at the left of the frequency axis gives the bandwidth of the chirped pulse. Note the much smaller frequency content of the bandwidth given by Eq. (1) as compared to the bandwidth given by the Fourier incertitude relation in the case of the shorter pulse.

or

$$\frac{\delta t}{\Delta T_0} \geq \sqrt{2} \sqrt{\frac{\Delta T}{\Delta T_0}}. \tag{4}$$

One can think of the δt inequality as a *localization criterion.* Indeed, for a short pulse of duration δt_1 much smaller than δt (see left of the time axis in Fig. 1), the perturbation spectral bandwidth $d\omega_1$ becomes very much larger than $\Delta\omega_1$ given by $\Delta\omega_1 = a \times \delta t_1$. There is no more a direct relation between the instantaneous frequency and time because sharp transients produce spectral modulations which extend all over the pulse bandwidth. We note that in previous experiments using single-shot chirped-pulse FDI (Benuzzi-Mounaix *et al.*, 1999; Chien *et al.*, 1999), the localization criterion was satisfied for the time scale of the probe pulse perturbations but the claimed ultimate temporal resolution (Chien *et al.*, 1999) was questionable on the basis of the simple interpretation of the time-frequency relation (Rebibo *et al.*, 2000). As stated before, this is because time and frequency are intertwined in the signal through the linear chirp [see Eq. (1)].

2.2. Reconstruction procedure

To overcome the resolution limitation due to the localization criterion, we have devised a retrieving procedure which unfolds the linear chirp from the frequency spectrum, allowing us to recover the full time resolution associated with the bandwidth $\Delta\Omega$ of the probe pulse. At this point, we assume that we have a signal processing technique which allows us to extract the complex perturbation of the probe signal

https://doi.org/10.1017/S026303460119110X Published online by Cambridge University Press

(Lepetit, 1997; Dorrer *et al.*, 2000). We note that FDI can work equally well in reflection from, or transmission through, the perturbed media. We thus write this complex perturbation in the frequency-domain as

$$P(\omega) = \sqrt{R(\omega)}\exp(j\Delta\Phi(\omega)), \tag{5}$$

where $R(\omega)$ can be thought of as a (intensity) reflection coefficient and $\Delta\Phi(\omega)$ a phase shift difference between the perturbed and unperturbed sample. With the knowledge of the chirp parameter a, which can be obtained from the known grating distance detuning or be determined experimentally, the original time resolution can be recovered. The field of the chirped-pulse can be written in the frequency domain:

$$E_0(\omega) = \mathcal{E}_0(\omega)\exp(j(\omega-\omega_0)^2/a). \tag{6}$$

We construct the signal by multiplying Eq. (5) by Eq. (6), so that

$$E(\omega) = E_0(\omega) \times P(\omega). \tag{7}$$

The field perturbation $P(t)$ in the time domain can be now easily recovered by using an inverse-Fourier-transform:

$$P(t) = \mathcal{F}^{-1}[E(\omega)]/E_0(t), \tag{8}$$

where $E_0(t)$ is the original chirped-pulse in the time-domain.

Because one wants to cover the largest time interval of the perturbation in a single shot, the major limitation of the chirped-pulse technique, even with the use of the reconstruction procedure, lies in the spectral resolution of the spectrometer. Indeed, the useful spectral range is practically limited to the spectral width at about $I(\omega_0)/4$ to avoid excessive noise. To ensure a spectral phase variation (associated to the chirp) of less than say, one radian, between to adjacent resolution points (i.e., pixels) near the clipping frequencies, one has to use a minimum number of resolution points (Rebibo, 2000) of about

$$N_{min} \approx 8\ln 2\,\frac{\Delta T}{\Delta T_0}. \tag{9}$$

This means that to cover a temporal range of 100 times the compressed probe pulse duration, one has to use about 500 points of resolution. However, one has to keep in mind that the number of shots required to acquire the same information is also divided by 100 when compared to the original FDI technique (Geindre *et al.*, 1994).

In FDI, phase differences $\Delta\Phi(\omega)$ and amplitude ratios $R(\omega)$ are determined by comparing the results of a signal shot and of a reference shot (with the pump pulse removed). Accordingly, there are basically two classes of frequency-domain interferometers, one which uses a time-delayed reference, and one which uses a space-shifted reference. In the twin-probe configuration (two time-delayed pulses), the fringe spacing is determined by the temporal delay between the two pulses. The fringes are along the spectral axis in this configuration. According to Eq. (9), to resolve tiny fringe shift variations, one has to use a very high resolution spectrometer with a detector having a large number of resolution points. In the space-shifted FDI technique, like the Mach–Zehnder configuration to be described below, fringes are obtained in the spatial domain by tilting the two interfering probe pulse wavefronts. The fringes are in a direction perpendicular to the spectral axis in this configuration. This greatly relaxes the spectral resolution constraint, providing the bandwidth coverage described above is preserved. Indeed, the fringe separation is now related to the angle of the two beam wavefronts and can be chosen so as to match the detector resolution. Moreover, in the context of dual-quadrature FDI (Quoix *et al.*, 1999), S- and P-polarization probe beams can be separated and shifted in the two arms of the interferometer. After projection of the two polarization components along their bisector with a polarizer, the P-polarized perturbed beam interfere with the S-polarized unperturbed beam and vice-versa, as depicted in Figure 2.

2.3. Experimental setup

Part of the experiments were performed at Laboratoire d'Optique Appliquée (LOA) with the Titane:Sapphire CPA laser capable of delivering 10-Hz, 35-fs, 150-mJ pulses at 0.82-μm wavelength. A main beam is focused on target with a mirror parabola of 1-m focal length at an incidence angle of 51.5° with respect to the target normal (see Fig. 3). The intensity contrast ratio of the beam is about 10^6. A weak probe beam, frequency doubled to 0.41-μm wavelength, is focused on target with a MgF_2 lens of 1.5-m focal length, so that its focal spot size is very much larger than the 60-μm pump focal spot. This is mandatory to allow interferences between perturbed and unperturbed regions of the target (see Fig. 2). The 35-fs probe pulse was stretched to typical values of 3 ps by slightly detuning the pulse compressor gratings. The P-polarization of the probe beam is rotated by 45° with respect to the plane of incidence with a half-wave plate. After reflection from the target, the probe focal spot is imaged (magnification ratio of 3.5) on the entrance polarization separation prism of the Mach–Zehnder. The interferometer is globally set with equal arm path lengths but the beam wavefront are slightly tilted and shifted so as to reproduce the spatial overlap depicted in Figure 2. The beams are then recombined in a second prism, and their polarization

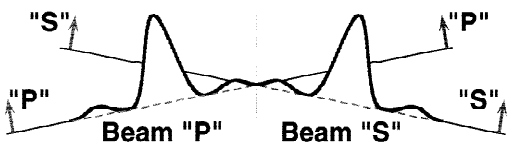

Fig. 2. Schematic view of the tilted and shifted wavefronts in the Mach–Zehnder configuration.

https://doi.org/10.1017/S026303460119110X Published online by Cambridge University Press

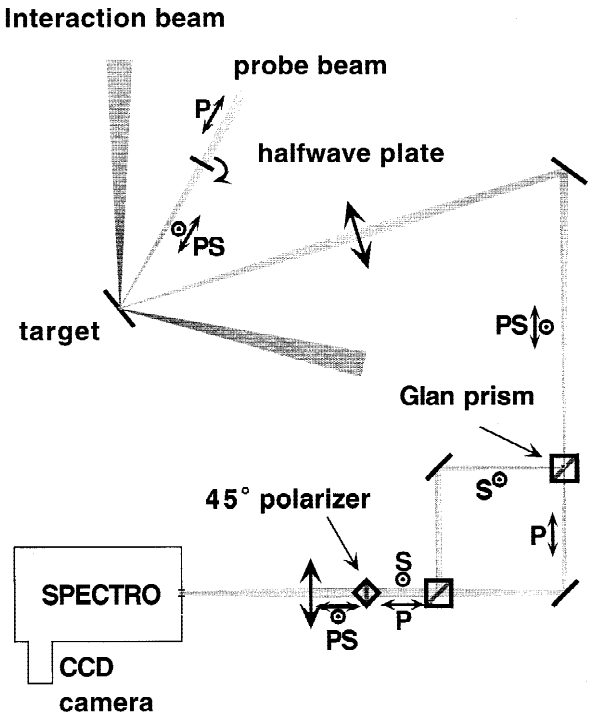

Fig. 3. Experimental setup showing the pump and probe beams configuration, the Mach–Zehnder interferometer, and the combination of the spectrometer and the CCD detector.

is projected along their bisector to allow the formation of interference fringes. The entrance prism is imaged again (magnification ratio of 4) on the entrance slit of a 1-m homemade Czerny–Turner spectrometer. A 16-bits charge-coupled-device (CCD) camera records the spectrum. A similar system was also installed at the Laboratoire d'Utilisation des Lasers Intenses (LULI) with a Nd:glass CPA laser delivering 350-fs, 10-J pulses at 1.06-μm wavelength. In both installations, temporal characterization of the various laser pulses was performed by autocorrelation and cross-correlation techniques, such as the SPIDER technique (Dorrer, 1999).

3. EXPERIMENTAL RESULTS

Figure 4 shows a raw spectrum obtained with a C_3H_6 target. Around the position of the S-polarized image of the pump focal spot, one can clearly see the fringe shift for the different wavelengths and the straight, unperturbed, fringes in the periphery of the S-focal spot. The situation is more complicated around the center of the P-polarized image of the focal spot. Strong modulations appear which can be explained by the generation of the second harmonic (SHG) of the pump beam scattered off the target, that is, at the same wavelength as the probe beam. This radiation interferes with the probe beam to give rise to spectral fringes. Because SHG is a nonlinear process, the duration of the corresponding emission is very short, commensurable with the pump pulse duration. We note that for these fast modulations to be resolved, one needs a good spectral resolution. In practice, this "parasitic" signal is very useful in determining the origin of the time scale of the experiment, that is, the time of the peak of the pump laser pulse.

Both P- and S-polarization focal spot images are processed to get the complex response of the perturbation, that is, the phase shift difference $\Delta\Phi(\omega)$ and the reflection coefficient $R(\omega)$. Starting from the image shown in Figure 4, we perform a line-out parallel to the horizontal axis (i.e., at a given probe wavelength). The spectral power $I(x)$ can be written

$$I(x) = |f(\omega)|^2\left(1 + R(x)^2 + 2R(x)\cos\left(\frac{2\pi x}{d} + \Phi(x)\right)\right), \quad (10)$$

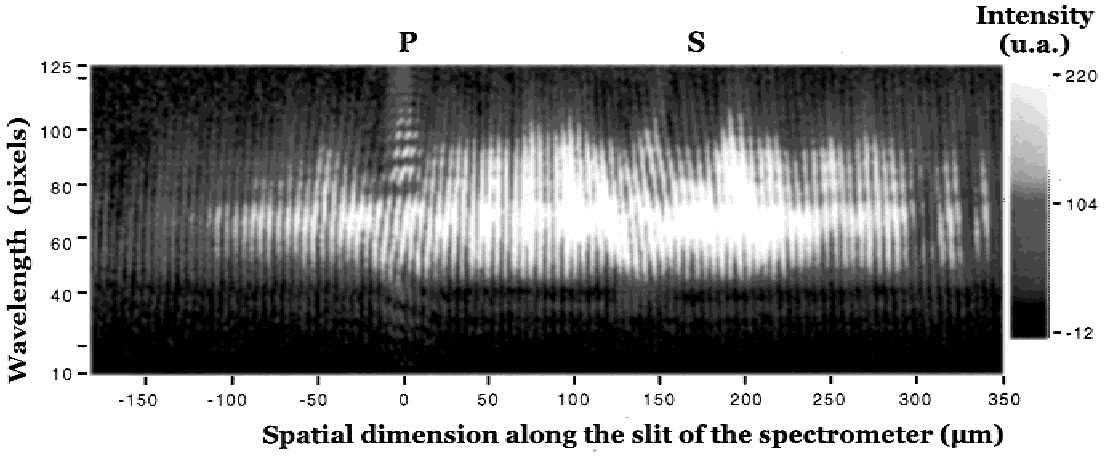

Fig. 4. Raw spectral interferogram recorded on the CCD camera. The spectral axis is vertical and the spatial fringe direction, which is also the direction of the spectrometer entrance slit, is horizontal. The spatial origin is arbitrarily at the center of the P-polarized focal spot.

https://doi.org/10.1017/S026303460119110X Published online by Cambridge University Press

where $R(x)$ and $\Phi(x)$ are the reflection coefficient and the phase difference to be determined, respectively, and d is the unperturbed interfringe distance, determined by the tilting angle of the Mach–Zehnder. The inverse Fourier–transform of $I(x)$ shows three peaks in the k domain, the two interesting (oscillating) peaks are located at $\pm k_0 = (2\pi)/d$. Isolating one of the lateral peaks and performing the Fourier transform back into the x-domain on both the signal shot and the reference shot, we get

$$I_S(x) = |f(\omega)|^2(R(x)\exp(ik_0x + \Phi(x))) \quad (11)$$

$$I_R(x) = |f(\omega)|^2(\exp(ik_0x)). \quad (12)$$

From the ratio of these quantities, we get easily the complex reflection coefficient perturbation. We note that the above signal processing is very general and has been applied, for example, to measure the spatial variation of the density in pulsed gas jets (Malka *et al.*, 2000).

Using a polypropylene target (C_3H_6) irradiated at a laser intensity of 10^{17} W/cm^2, we have obtained the reflection coefficient and the phase shift of a chirped-pulse probe stretched to 2.8 ps, centered on the 35-fs pump pulse. Figure 5 gives the results taken at a distance of 100 μm from the center of the focal spot. Equivalent planes images of the focal spot suggest that the intensity is about four orders of magnitude lower than at the peak, that is, $\approx 10^{13}$ W/cm^2. The rapid phase jump is the signature of laser breakdown at the surface of the target (Quoix *et al.*, 1999). The delay between the onset of the phase variation and the reflectivity variation is easily explained, within the framework of the Drude model, by the greater sensitivity of the phase (real part of the dielectric constant) to the electron density rise during the transient ionization (Quoix *et al.*, 1999). We clearly demonstrate the benefit of the reconstruction procedure in obtaining a temporal resolution which is close to the compressed probe pulse duration. Indeed, the rise time of the reflectivity signal is below 50 fs.

The previous results were obtained in one shot (in fact two shots, including the reference shot) at the LOA laser facility. Because this laser is capable of a repetition rate of 10 Hz, the present single-shot technique is not indispensable for doing pump/probe measurements. The decisive advantage of the present technique manifests fully its strength with large energy Nd:glass lasers, with repetition rates of one shot every 20 mn or more. This is the case of the LULI 100-TW laser (Gauthier *et al.*, 1999) where we have conducted a study of the weak plasma generated by controlled prepulses. Engineering the electron density gradient scale length is a common problem in X-ray laser research (MacPhee *et al.*, 1997), ultrafast incoherent X-ray production (Bastiani *et al.*, 1999), and high-intensity laser ion acceleration (Rosmej *et al.*, 1999). We have irradiated pure carbon targets at rather low irradiances of about 2×10^{15} W/cm^2 with 350-fs duration, frequency-doubled (0.53-μm) laser pulses at 60° incidence angle. The probe beam at 1.06 μm was stretched to 20 ps. Its incidence angle (20°) was chosen so that the critical density associated with the probe beam was close to the critical density of the pump beam. Here, the phase shift in S- and P-polarization was

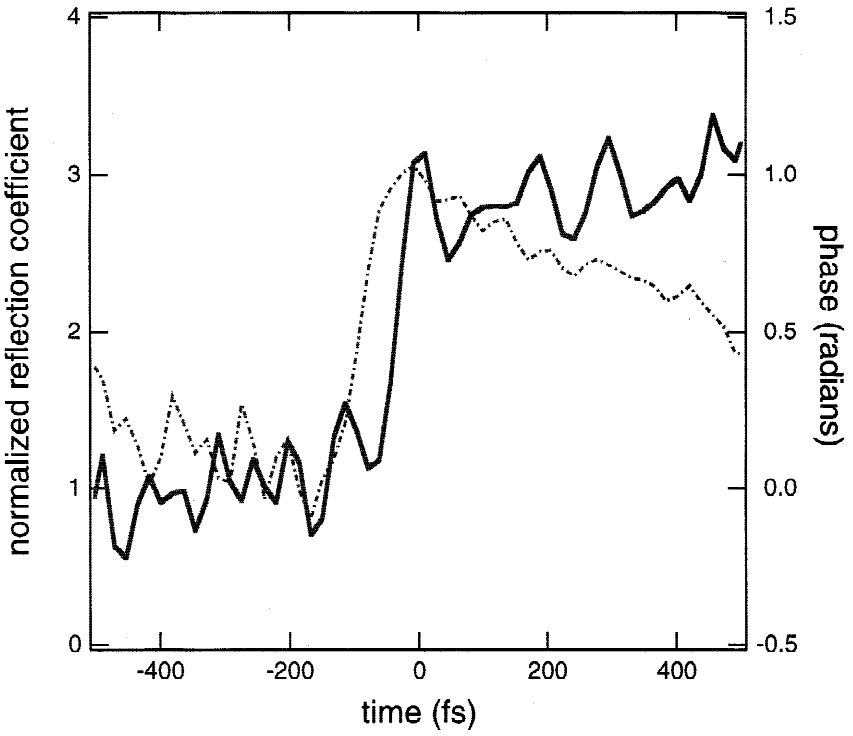

Fig. 5. P-polarized probe pulse phase shift and reflectivity as a function of time for a C_3H_6 target. Results obtained with the 35-fs duration LOA laser. Laser intensity at the measurement point is about 10^{13} W/cm^2.

https://doi.org/10.1017/S026303460119110X Published online by Cambridge University Press

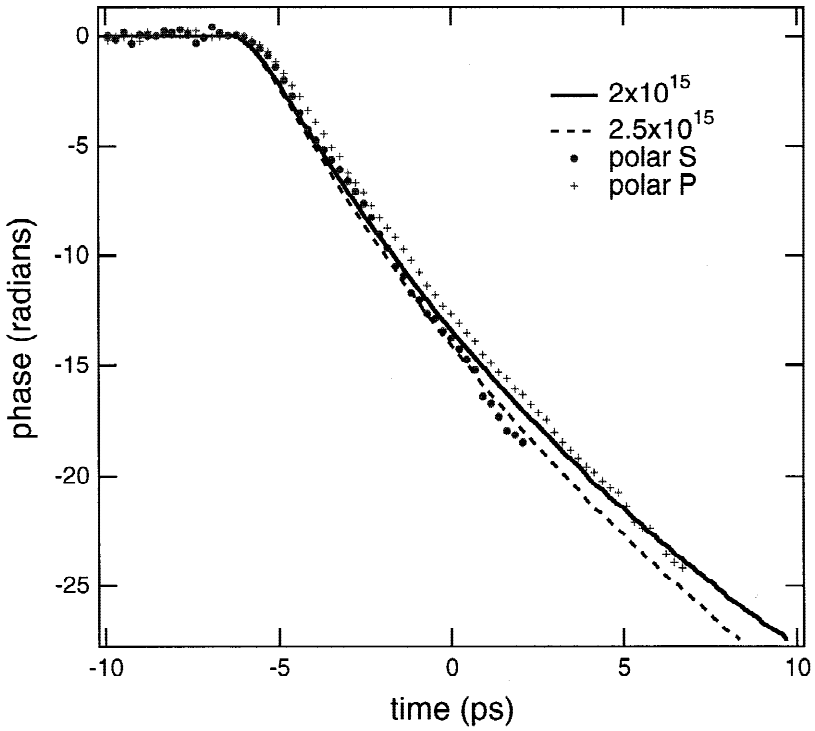

Fig. 6. Phase shift of P- and S-polarized probe beams as a function of time following the interaction of a pure carbon target with the 350-fs duration LULI laser pulse. Circles, S-polarization; crosses, P-polarization. Hydrocode results for S-polarization and for two intensities are shown for comparison.

followed over about 15 ps as shown in Figure 6. It has been previously shown that the late phase shift variation of a probe beam on a plasma is due to the motion of the reflection turning point, providing the Doppler velocity of the critical density front (Blanc *et al.*, 1996). This Doppler phase is independent to first order on the polarization state of the probing light, as verified in Figure 6. Experimental results are compared with the predictions of the FILM hydrocode, which has been adapted to the treatment of ultrafast laser interaction (Teubner *et al.*, 1996). Here the code was run at an irradiance of 2×10^{15} W/cm^2 and 2.5×10^{15} W/cm^2 to show the sensitivity of the measurement method. We have a good agreement which shows the precision and the usefulness of the method to characterize the scale length of prepulse-induced electron density gradients.

4. CONCLUSIONS

In conclusion, we have introduced a new type of *single-shot* frequency-domain interferometer based on a Mach–Zehnder configuration. It allows us to perform dual-quadrature phase and amplitude measurements of the perturbation of a chirped-probe pulse interacting with a plasma in reflection. Extension of this technique to other interaction geometries (transmission) or samples (gas jets) is straightforward. The interferometer provides spatial resolution along a line-out of the focal spot. The spectral resolution requirements have been shown to be less stringent than in double-pulse FDI, especially with chirped pulses. Various aspects on the time resolution of such devices have been discussed. The direct interpretation of the spectra based on the linear encoding of time into frequency has been shown to lead to systematic errors in the dynamics of the retrieved spectral phase differences. We have proposed and demonstrated a reconstruction technique which allows us to recover the temporal resolution associated with the full bandwidth of the probe pulses.

The new interferometer has been used in two types of experiments:

- Laser breakdown of a dielectric target with the potential of exploiting the very short pulse duration of the LOA laser (35 fs) for obtaining a spatially and temporally resolved assessment of the contrast quality of ultrafast pulses.
- Precise characterization of the plasma created by prepulses in the context of laser interaction research with high energy lasers such as the LULI laser where the single-shot capability of the instrument is fully exploited.

REFERENCES

Audebert, P., Daguzan, P., Dos Santos, A., Gauthier, J.-C., Geindre, J.-P., Guizard, S., Hamoniaux, G., Krastev, K., Martin, P., Petite, G. & Antonetti, A. (1994). *Phys. Rev. Lett.* **73**, 1990.

Bastiani, S., Audebert, P., Geindre, J.-P., Schlegel, Th., Gauthier, J.-C., Quoix, C., Hamoniaux, G., Grillon, G. & Antonetti, A. (1999). *Phys. Rev. E* **60**, 3439.

Benuzzi-Mounaix, A., Koenig, M., Boudenne, J.-M., Hall, T., Scianitti, F., Masini, A. & Batani, D. (1999). *Phys. Rev. E* **60**, R2488.

Blanc, P., Audebert, P., Falliès, F., Geindre, J.-P., Gauthier, J.-C., Dos Santos, A., Mysyrowicz, A. & Antonetti, A. (1996). *J.O.S.A. B* **13**, 118.

https://doi.org/10.1017/S026303460119110X Published online by Cambridge University Press

Chien, C.Y., La Fontaine, B., Desparois, A., Jiang, Z., Johnston, T.W., Kieffer, J.-C., Pépin, H. & Vidal, F. (1999). *Opt. Lett.* **25**, 578.

Dorrer, C. (1999). *Opt. Lett.* **24**, 1532.

Dorrer, C., Belabas, N., Likforman, J.-P. & Joffre, M. (2000). *Appl. Phys. B* **70**, 99.

Evans, R., Badger, A.D., Falliès, F., Mahdieh, M., Hall, T., Audebert, P., Geindre, J.-P., Gauthier, J.-C., Mysyrowicz, A., Grillon, G. & Antonetti, A. (1996). *Phys. Rev. Lett.* **77**, 3359.

Froehly, C., Lacourt, A. & Viénot, J.-C. (1973). *J. Opt. (Paris)* **4**, 183.

Gauthier, J.-C., Amiranoff, F., Chenais-Popovics, C., Jamelot, G., Koenig, M. Labaune, C., Leboucher, E., Sauteret, C. & Migus, A. (1999). *Laser Part. Beams* **17**, 195.

Geindre, J.-P., Audebert, P., Rousse, A., Falliès, F., Gauthier, J.-C., Mysyrowicz, A., Dos Santos, A., Hamoniaux, G. & Antonetti, A. (1994). *Opt. Lett.* **19**, 1997.

Gold, D., Sullivan, A., Dunn, J., Shepherd, R. & Stewart, R. (1996). Paper presented at the International Seminar on Physics of High Energy Matter, Vancouver, Canada (unpublished).

Guizard, S., Martin, P., Daguzan, Ph., Petite, G., Audebert, P., Geindre, J.-P., Dos Santos, A. & Antonetti, A. (1995). *Europhys. Lett.* **29**, 401.

Lepetit, L. (1997). *Optique non-linéaire à deux dimensions spectrales.* Ph.D. thesis, Ecole polytechnique (available upon request to the authors).

Lepetit, L., Chériaux, G. & Joffre, M. (1995). *J.O.S.A. B* **12**, 2467.

MacPhee, A.G., Lewis, C.L.S., Warwick, P.J., Weaver, I., Jaeglé, P., Carillon, A., Jamelot, G., Klisnick, A., Rus, B., Zeitoun, Ph., Nantel, M., Goedkindt, P., Sebban, S., Tallents, G.J., Demir, A., Holden, M. & Krishnan, J. (1997). *Optics Commun.* **133**, 525.

Malka, V., Coulaud, C., Geindre, J.P., Lopez, V., Najmudin, Z., Neely, D. & Amiranoff, F. (2000). *Rev. Sci. Instrum.* **71**, 2329.

Marquès, J.-R., Geindre, J.-P., Amiranoff, F., Audebert, P., Gauthier, J.-C., Antonetti, A. & Grillon, G. (1996). *Phys. Rev. Lett.* **76**, 3566.

Piasecki, J., Colombeau, B., Vampouille, M., Froehly, C. & Arnaud, J.A. (1980). *Appl. Opt.* **19**, 3749.

Quoix, C., Grillon, G., Antonetti, A., Geindre, J.-P., Audebert, P. & Gauthier, J.-C. (1999). *EPJ: Applied Physics* **5**, 163.

Quoix, C., Hamoniaux, G., Antonetti, A., Gauthier, J.-C., Geindre, J.-P. & Audebert, P. (2000). *J. Quant. Spectr. Radiat. Transfer* **65**, 455.

Rebibo, S. (2000). *Interférométrie spectrale à haute résolution d'un plasma créé par une impulsion de 35 fs.* Ph.D. thesis, Ecole polytechnique (available upon request to the authors).

Rebibo, S., Geindre, J.-P., Audebert, P. & Gauthier, J.-C. (2000). Submitted for publication.

Rosmej, F., Hoffmann, D., Geissel, M., Pirzadeh, P., Roth, M., Seelig, W., Faenov, A.Ya., Skobelev, I.Yu., Magunov, A.I., Pikuz, T.A., Bock, R., Funk, U.N., Neuner, U., Udrea, S., Tauschwitz, A., Tahir, N.A., Sahrkov, B.Yu. & Andreev, N.E. (1999). *JETP Letters* **70**, 270.

Scherer, N., Carlson, R., Matro, A., Du, M., Ruggiero, A., Romero-Rochin, V., Cina, J., Fleming, G. & Rice, S. (1991). *J. Chem. Phys.* **95**, 1487.

Siders, C., Le Blanc, S., Fisher, D., Tajima, T., Downer, M., Babine, A., Stepanov, A. & Sergeev, A. (1996). *Phys. Rev. Lett.* **76**, 3570.

Strickland, D. & Mourou, G. (1985). *Opt. Lett.* **56**, 219.

Teubner, U., Gibbon, P., Förster, E., Falliès, F., Audebert, P., Geindre, J.-P. & Gauthier, J.-C. (1996). *Phys. Plasmas* **3**, 2679.

Tokunaga, E., Terasaki, A. & Kobayashi, T. (1992). *Opt. Lett.* **17**, 1131.

https://doi.org/10.1017/S026303460119110X Published online by Cambridge University Press